







Low-temperature polycrystalline silicon waveguides for low loss transmission in the near-to-mid-infrared region

AMAR N. GHOSH,^{1,*}  STUART J. MACFARQUHAR,¹
OZAN AKTAS,^{1,2}  THAN S. SAINI,¹  SWE Z. OO,³ 
HAROLD M. H. CHONG,^{3,4}  AND ANNA C. PEACOCK¹ 

¹Optoelectronics Research Centre, University of Southampton, Highfield, Southampton, SO17 1BJ, UK

²Cambridge Graphene Centre, University of Cambridge, 9 JJ Thomson Avenue, Cambridge, CB3 0FA, UK

³School of Electronics and Computer Science, University of Southampton, Highfield, Southampton, SO17 1BJ, UK

⁴School of Materials Science, Japan Advanced Institute of Science and Technology, Nomi, Ishikawa 923-1292, Japan

*A.N.Ghosh@soton.ac.uk

Abstract: Low-temperature deposited polycrystalline silicon waveguides are emerging as a flexible platform that allows for dense optoelectronic integration. Here, the optical transmission properties of poly-silicon waveguides have been characterized from the near-to-mid-infrared wavelength regime, extending the optical transmission well beyond previous reports in the telecom band. The poly-Si waveguides with a dimension of $3\ \mu\text{m} \times \sim 0.6\ \mu\text{m}$ have been produced from pre-patterned amorphous silicon waveguides that are post-processed through laser melting, reflowing, and crystallization using a highly localized laser induced heat treatment at a wavelength of 532 nm. Low optical transmission losses ($< 3\ \text{dB cm}^{-1}$) have been observed at $1.55\ \mu\text{m}$ as well as across the wavelength range of $2\text{--}2.25\ \mu\text{m}$, aided by the relatively large waveguide heights that are enabled by the deposition process. The results demonstrate the suitability of low-temperature poly-silicon waveguides to find wide ranging applications within integrated mid-infrared systems.

Published by Optica Publishing Group under the terms of the [Creative Commons Attribution 4.0 License](https://creativecommons.org/licenses/by/4.0/). Further distribution of this work must maintain attribution to the author(s) and the published article's title, journal citation, and DOI.

1. Introduction

Silicon photonics is fast becoming an established platform for the development of high performance, high density optical circuits that have the potential to be integrated with silicon electronic layers [1–3]. Using traditional silicon-on-insulator (SOI) substrates and CMOS processing technologies, an extensive range of integrated photonic devices with outstanding performance metrics have been realized [4–6]. Although single crystal silicon platforms offer low losses and excellent electronic properties, they present several challenges when considering integration with electronic layers, as well as for the development of space saving 3D photonic circuits [7,8]. Alternatively, polycrystalline silicon (poly-Si) materials that can be deposited at low temperatures are emerging as a complementary platform that offer much more flexibility in terms of multi-layer integration, but yet still preserve key features of the single crystalline materials such as good electron mobility and power stability when compared to amorphous material [9–11]. Provided the polycrystalline materials can be produced with grain sizes that are approaching typical device lengths, the optoelectronic properties can be comparable to their SOI counterparts, allowing for the development of high quality passive and active poly-Si devices [12].

As of to date, a variety of techniques have been applied to post-process the low temperature deposited poly-Si waveguides to increase the grain size and thus reduce the optical losses down

to practical levels, including thermal annealing [13] and laser heat treatments [9]. Most recently, we have reported the production of poly-Si waveguides by post-processing low temperature deposited amorphous waveguides with a continuous wave (CW) laser to obtain transmission losses as low as 4 dB cm^{-1} [14], which are close to the loss values of c-Si waveguides with similar dimensions. Despite the promising progress that has been made in poly-Si material development, so far all of the attention has focused on the characterization and application of the devices in the near-infrared region, primarily over the telecommunications bands [10,14]. However, if the operation window can be extended to longer mid-infrared wavelengths ($>2 \mu\text{m}$), the application potential for the poly-Si waveguides will reach into new areas such as bio-chemical sensing, spectroscopy and free-space communications [15–17].

In this work, we investigate the fabrication and characterization of CW laser processed poly-Si waveguides for application at wavelengths $>2 \mu\text{m}$. The poly-Si waveguides are produced from pre-patterned amorphous silicon waveguides, followed by laser melting, reflowing, and crystallization through localized CW laser processing at a wavelength of 532 nm. Raman measurements have been used to confirm the crystallization of the waveguides, with good crystallinity being reported along the lengths. Wavelength dependent loss measurements show that the losses of the waveguides remain low ($<3 \text{ dB cm}^{-1}$) from $1.55 \mu\text{m}$ up to $2.25 \mu\text{m}$, indicating that the reshaping of the surface is advantageous for supporting propagation over the longer wavelength regions. We expect these results to open up new opportunities for the flexible integration of poly-Si waveguides into high performance systems operating from the near to mid-infrared spectral regions.

2. Fabrication of polysilicon waveguide

Polycrystalline silicon (poly-Si) waveguides are fabricated in two principal steps. The first step includes the fabrication of amorphous silicon waveguides using chemical vapour deposition (CVD) and electron beam (e-beam) lithography techniques. The second step includes the post-process laser reflowing of the previously fabricated amorphous silicon waveguides using a high power CW laser. The two above mentioned steps will be discussed briefly in the following sections.

2.1. Fabrication process of amorphous silicon waveguide

In this work, a hot-wire CVD (HWCVD) process was used to deposit a 400 nm thick amorphous silicon (a-Si) layer on a $5 \mu\text{m}$ thick optically isolating SiO_2 buried-oxide layer using a silane (SiH_4) precursor. The buried oxide layer was grown by wet thermal oxidation on the top of a 1 mm thick crystalline silicon (c-Si) wafer in the initial stage [18]. The HWCVD process was chosen over other low-pressure and plasma enhanced CVD techniques due to the fact that it allows us to deposit a-Si, with low hydrogen concentration, at a substrate temperature as low as 230°C to produce CMOS compatible devices [19–22]. Minimizing the hydrogen content through the adjustment of gas pressure is important as it helps to eliminate any possibility of violent out-diffusion during the laser post-processing. Using a pressure of 0.01 mbar and silane gas flow of 40 sccm, the a-Si layer was deposited at a rate of 0.69 nm s^{-1} . After the deposition was performed, e-beam lithography and inductively-coupled plasma reactive ion etching (ICP-RIE) were used to pattern the 400 nm thick a-Si thin film into straight waveguides with a width of $3 \mu\text{m}$ as shown in Fig. 1. Waveguide widths as large as $3 \mu\text{m}$ were chosen as they are well suited to confining longer wavelength light for mid-infrared transmission, as explained in Section 2.2.

2.2. Post-process laser reflowing of amorphous silicon waveguide

This section describes the laser processing of the pre-patterned a-Si waveguides, reported in our previous works [12,14]. The schematic of the experimental setup used for laser processing is demonstrated in Fig. 2(a). For the laser source, we used a single frequency and highly stable green

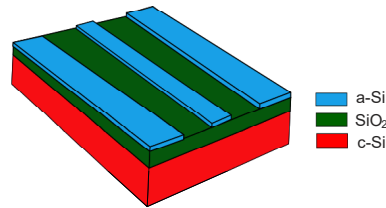


Fig. 1. Schematic of a-Si waveguide after patterning. The thickness of c-Si, SiO₂ and a-Si are 1 mm, 5 μm, and 400 nm, respectively.

fiber laser (IPG-GLR-10W) emitting continuous-wave (CW) radiation at 532 nm with a maximum power of 10 W. Pre-patterning of the a-Si waveguides reduces the laser processing area and enables confinement of the thermal energy during the process of laser melting and crystallization [12]. Therefore, it allows us to use a CW laser source for processing of these waveguides without overheating the substrate, which helps to improve the stability of the processing when compared to pulsed laser sources that have been more typically applied to large area crystallization [9,23]. Furthermore, the localized heating technique reduces the overall thermal budget of fabrication process and increases the grain growth by promoting directional solidification and liquid phase crystallization from the trailing edge of the continuously moving molten zone during the complete melting of the a-Si wire.

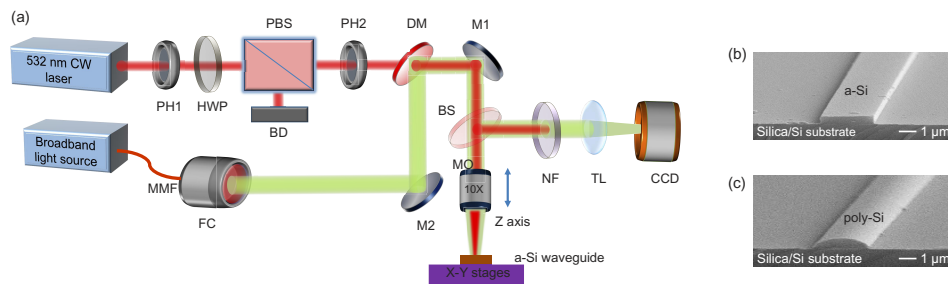


Fig. 2. (a) Schematic of the experimental setup for laser processing of a-Si waveguides. PH, pinhole; HWP, half-wave plate; PBS, polarization beam splitter; BD, beam dump; DM, dichroic mirror; M, mirror; BS, beam splitter; MO, microscope objective; MMF, multimode fiber; FC, fiber collimator; NF, notch filter; TL, tube lens. SEM image of (b) a-Si waveguide with a width of 3 μm and a height of 400 nm, before laser processing and (c) poly-Si waveguide with a width of 3 μm and an apex height of ~ 600 nm, after laser processing. The processing parameters were 285 mW of incident power at a scanning speed of 0.1 mm s⁻¹

The output power of the linearly polarized laser was initially fixed at its minimum value of 500 mW. A combination of half-wave plate and a polarization beam splitter was used after the laser to further reduce and adjust its power to the range of 10 – 295 mW, which was measured at the sample plane after the focusing microscope objective. The 10× microscope objective (NA = 0.3) focused the 1 mm laser beam on the top surface of the sample to produce a laser spot with a diameter of 13.5 μm, which was sufficient to cover the entire surface of our 3 μm wide a-Si waveguides. The sample waveguide chip was mounted with a vacuum holder on a software controlled two-axis (X/Y) high precision stage (Aerotech, ABL-1500) and the microscope objective was mounted on a high-precision z-axis stage. A broadband light source was coupled with the laser beam using a fiber collimator and dichroic mirror (transmits at the laser wavelength) to illuminate the sample surface. The reflected light from the sample surface was then used

to image the sample surface on a CCD camera through a 92 : 8 beam splitter and a tube lens. The adjustability of the tube lens ensured the independent movement of the laser focus and imaging focus. A notch filter before the tube lens was used to protect the CCD camera from laser light. The real-time imaging of our sample surface not only helped us with initial alignment and focusing of the laser beam but also allowed us to detect the partial melting or ablation of the material during laser processing of the waveguides.

Laser processing was performed by moving the sample-stage linearly at a constant speed to scan the 13.5 μm laser spot from one end to the other end of our 2-cm long a-Si waveguides. At first, several sections of a test waveguide were processed using parameters such as scan speed ranging from 0.1 mm s^{-1} to 1 mm s^{-1} and laser power ranging from 270 mW to 350 mW. The optimum parameters were determined after investigating both the surface and crystalline quality of the test waveguide sections using microscopy and Raman spectroscopy. Finally, the rest of the a-Si waveguides were processed with an incident optical power of 285 mW and a scan speed of 0.1 mm s^{-1} as shown in the scanning electron microscope images in Figs. 2(b),(c). During the laser processing, localized heating induced material reflow and surface tension reshaping of the molten silicon transforms the cross-section of the waveguide into a parabolic shape from its initial rectangular shape (see Fig. 2(c)). This cross-section reshaping introduced two changes in the poly-Si waveguide that are beneficial for mid-infrared waveguiding. Firstly, it helps to improve the surface quality of the waveguide, reducing the surface roughness down to 0.5 nm [12,14], which is important to reduce scattering losses at the longer wavelengths that interact more strongly with the boundaries. Secondly, the poly-Si waveguide height increases to ~ 600 nm from its initial height of 400 nm (confirmed by atomic force microscopy measurement, reported in our previous work [14]), which is better for confining the longer wavelength light. However, due to the higher poly-Si material density compared to a-Si, the overall cross-sectional area of the waveguide was slightly reduced, but this was compensated for by the large initial waveguide widths. Although the scan speeds employed in our processing are too slow for mass production, these could be increased by using higher power laser systems and ensuring that the energy transfer remains below the material damage threshold [12]. The flexibility of the processing also means that fabrication of poly-Si waveguides with larger or smaller dimensions, e.g., widths down to 500 nm for single-mode operation in the telecom band, can be fabricated. This opens a potential route to fabricate complicated structures like micro-ring resonators and Mach-Zehnder interferometers with a limitation in the separation distance of two adjacent components to few tens of nanometer.

3. Material characterization of polysilicon waveguide

A Raman spectrometer (Renishaw Invia) was used to investigate the crystalline quality of our laser-processed poly-Si waveguides before and after laser processing. A 532 nm Nd:YAG laser was used as the source and focused to a spot diameter of 1 μm on our waveguide sample with the help of a 50 \times microscope objective (NA= 0.75). The measurement was taken in the backscattered mode by collecting Raman photons using a silicon diffraction grating of 2400 lines/mm with a precision of 0.12 cm^{-1} at low laser power to prevent the penetration of focused laser beam into c-Si substrate. Figure 3(a) shows the measured normalized Raman spectra of the unprocessed a-Si waveguide (black) and a laser-processed poly-Si waveguide (red). The as-deposited layer displays a Raman spectrum consisting of several peaks, which are typical for a-Si with a broad peak centered at 480 cm^{-1} . On the other hand, the Raman spectrum of the poly-Si waveguide has a sharp Raman peak centered at 518.6 cm^{-1} , which is shifted to the left from the characteristic Raman peak centered at 520.6 cm^{-1} of an external reference c-Si, as shown in Fig. 3(b). This shift in the Raman peak in our poly-Si waveguide towards lower frequencies is caused by residual tensile stress present in the material after laser processing [24]. It is noted that the Raman output from the waveguide cannot be directly compared with the reference c-Si value since the measured peaks are a convolution of spectrometer's Gaussian profile and the Lorentzian profile of the

materials. Therefore, in Fig. 3(b), the c-Si reference peak was first fit using a Voigt function to account for the Gaussian broadening induced by the spectrometer optics and the Lorentzian material line shape with a linewidth of $\Gamma_0 = 2.7 \text{ cm}^{-1}$. The Lorentzian line shape of the poly-Si waveguide was then deconvolved from the experimental data. The linewidth of the Raman peak of our poly-Si waveguide was found to be $\Gamma = 3.1 \pm 0.1 \text{ cm}^{-1}$. We attribute the slightly larger linewidth when compared to the c-Si peak due to residual tensile strain in the waveguides associated with the melting and reshaping [25], as previous X-ray diffraction measurements have revealed that the crystal grain sizes in these waveguides are larger than the laser spot used for the Raman spectroscopy [12]. However, both the Raman peak position and the linewidth remained remarkably consistent when scanned along the length (variations much less than 1%), indicating that the crystallinity and strain remained uniform within the waveguides due to the thermal steady-state ensured through our constant scan speeds and stable laser power during the processing.

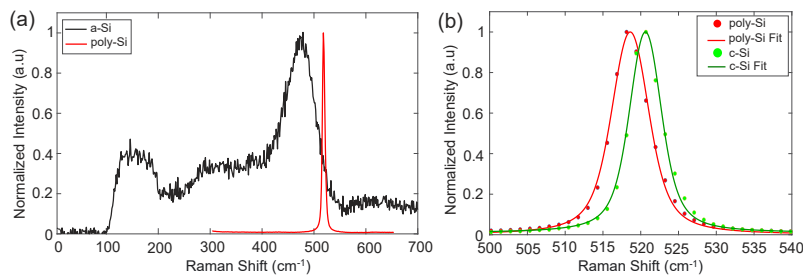


Fig. 3. Material characterization of a-Si and poly-Si waveguides using Raman spectroscopy. (a) The black and the red curve represent the Raman spectra of a-Si and poly-Si waveguides, respectively. (b) Comparison between poly-Si (red) and c-Si (green) Raman peaks. The Raman peak of the poly-Si waveguide is shifted and broadened slightly compare to the characteristic c-Si due to the residual tensile stresses after laser processing.

4. Wavelength dependent linear propagation loss in polysilicon waveguide

The principal motivation behind this work was the minimization of optical losses in our poly-Si waveguide. The characterization of the linear propagation loss in the poly-Si waveguide from the near-to-mid-infrared was carried out using the cut-back method by measuring the total losses at different lengths of the waveguide at a constant light injection condition. A schematic of the experimental setup used for the optical characterization is presented in Fig. 4. Two different light sources were used to cover the wavelength range. The first was a diode laser (Anritsu) emitting CW radiation at 1550 nm, delivered by a single mode fiber (SMF), with a maximum output power of 100 mW. The second was a free-space delivered single frequency $\text{Cr}^{2+}:\text{ZnS}/\text{Se}$ laser (IPG Photonics) tunable from 2 – 2.5 μm with a maximum output power of 3 W. The ZnS/Se laser was coupled into a 1 m long multimode fiber patch cable (Thorlabs, M43L01, 105 μm core diameter) and a variable attenuator was added in between to reduce the high power of the laser. Both facets of our $3 \mu\text{m} \times \sim 0.6 \mu\text{m}$ poly-Si waveguide were prepared by cleaving them with a ruby blade and inspected with a microscope for roughness and cleanliness. The sample waveguide chip was then placed on a 3-axis high-precision stage (Thorlabs, NanoMax-TS). TM polarized laser light was coupled into the waveguide using a 60 \times microscope objective (NA = 0.85) and waveguide alignment and light injection to the waveguide were monitored from the top using a home-built camera system consisting of an infrared (IR) camera (MicronViewer 7290A) with a sensitivity up to 1550 nm, attached to a Nikon microscope. The reason behind the fiberization of the ZnS/Se laser was to match the input light injection condition with the diode laser that helped us with

waveguide alignment and light injection to the waveguide from ZnS/Se laser. It was achieved by first aligning the waveguide with diode laser using the 1550 nm camera and then replacing the diode laser with ZnS/Se laser while keeping the same waveguide alignment. The output light from the waveguide was collected using a 25× microscope objective (NA = 0.5) and imaged on an another IR camera (MicronViewer 7290A) with an extended sensitivity up to 2.25 μm to investigate the mode profile. The collimated light from the collecting objective was then spatially filtered using a pinhole to isolate the mode and eliminate the scattered light as well as any light guided in the silica substrate. By carefully monitoring the input and output coupling using the IR camera with extended sensitivity, efficient coupling into the fundamental mode was achieved with both lasers, as can be seen from the far field image at 1.55 μm in Fig. 5(a) and at 2 μm in Fig. 5(b). Figures 5(c),(d) presents the calculated TM electric field amplitude for the fundamental mode of the waveguide at the wavelengths of 1.55 μm and 2 μm, respectively. The output power of the waveguide was measured after the pinhole with a power meter (Thorlabs, S140C).

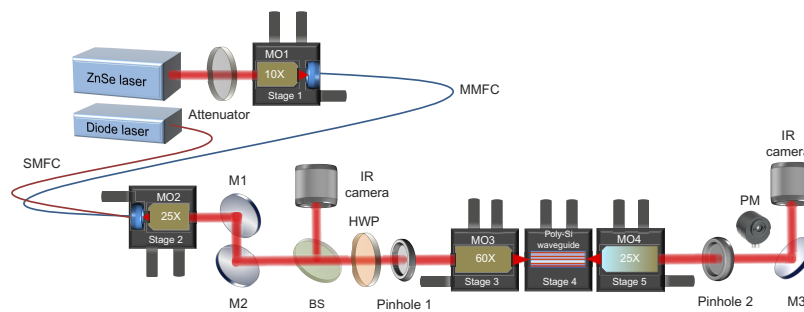


Fig. 4. Schematic of the experimental setup for characterization of the optical losses in the laser-processed poly-Si waveguides. MO, microscope objective; MMFC, multimode fiber connector; SMFC, singlemode fiber connector; M, mirror; BS, beam splitter; HWP, half-wave plate; PM, power meter.

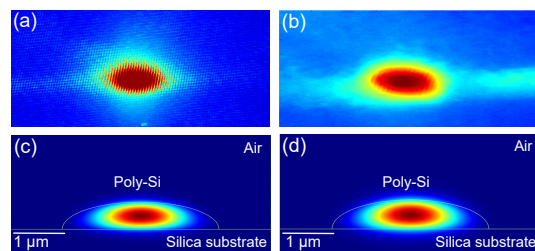


Fig. 5. Mode profiles of a poly-Si waveguide with a width of 3 μm and a height of ~ 600 nm. Experimentally obtained far field image at the output facet of the waveguide at (a) 1.55 μm and (b) 2 μm, taken using an IR camera. Calculated electric field amplitude for the fundamental TM mode at (c) 1.55 μm and (d) 2 μm. The effective refractive indices for the fundamental TM mode at 1550 nm and 2000 nm are 3.271 and 3.155, respectively.

Finally, cut-back measurements were performed by cleaving the waveguide sample at two different lengths from the output facet end (keeping the input facet intact). The transmission was recorded as a function of waveguide length using a 1550 nm laser, while ensuring an approximate consistent coupling condition at each measurement step by obtaining a similar cleave quality, with minimum roughness of the output surface, at the different waveguide lengths. Significantly, due to the parabolic cross section of the waveguides, and the high width-to-height aspect ratio, the TE and TM polarized modes have different propagation characteristics, so that the light propagation

is polarization-dependent. As the TM mode was found to have a lower propagation loss compared to the TE mode, our propagation loss measurements focused on the TM mode. The measurement results are shown in Fig. 6(a), where the total optical loss includes coupling losses at the front and end facets and propagation loss. The total coupling loss is 32.6 ± 0.5 dB, calculated from the y-intercept of the linear fits to the data. Lower coupling loss could be achieved by further minimizing the roughness of the cleaved surface and achieving better matching of the mode size and position at the input facet. The propagation loss for the TM mode as calculated from the slope of the transmission data for the $3 \mu\text{m}$ poly-Si waveguide was found to be $2.4 \pm 0.1 \text{ dB cm}^{-1}$ at $1.55 \mu\text{m}$. The error in the propagation loss was determined from the linear fit to the total loss data. The error in coupling loss is calculated from the uncertainty in the y-axis intercept. This propagation loss represents a significant reduction over our previous report of 4 dB cm^{-1} in the telecom band, which we attribute to further improvement of the stability of the setup that allowed us to work with lower powers and slower processing speeds [14]. Following this observation, further cut-back measurements were performed using the tunable ZnS/Se laser and the coupling loss and propagation loss were found to be $35.65 \pm 1 \text{ dB}$ and $2.9 \pm 0.24 \text{ dB cm}^{-1}$, respectively, at $2.15 \mu\text{m}$, as calculated from Fig. 6(b). Figure 6(c) then shows the wavelength dependent propagation loss measured by tuning the ZnS/Se laser wavelength from $2 - 2.25 \mu\text{m}$, where the upper wavelength was only limited by the sensitivity of our IR camera used for optimum coupling into the fundamental mode. The propagation loss of our poly-Si waveguide stays below 3 dB cm^{-1} in the telecom band as well as in the $2 - 2.25 \mu\text{m}$ region, indicating the potential of low temperature produced poly-Si waveguides to find use in applications ranging from the near-to-mid-IR regime. Moreover, thanks to the flexibility of the deposition process, it would be straightforward to fabricate poly-Si waveguides with larger vertical dimensions to extend the low loss transmission over even longer wavelengths.

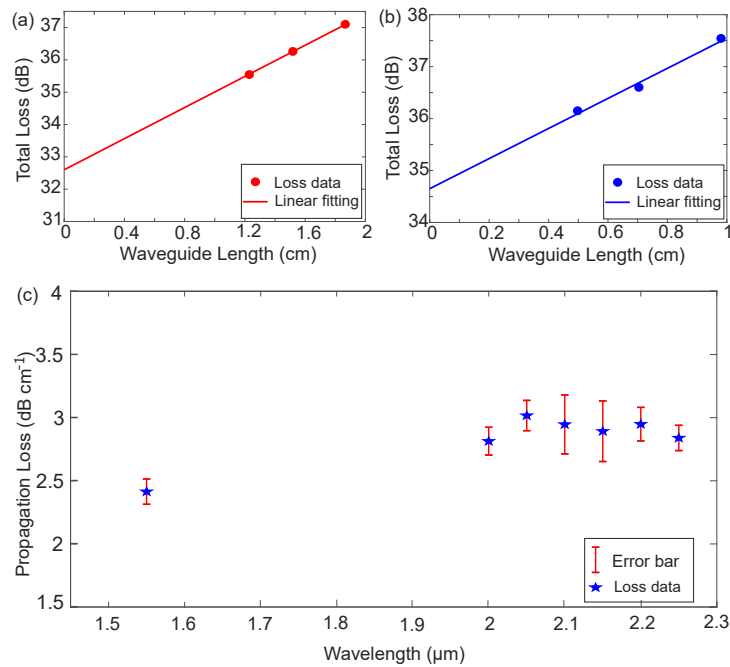


Fig. 6. Linear loss measurement of a poly-Si waveguide with a width of $3 \mu\text{m}$. Cut-back measurements for (a) $1.55 \mu\text{m}$ and (b) $2.15 \mu\text{m}$ laser sources, revealing propagation losses of 2.4 dB cm^{-1} and 2.9 dB cm^{-1} , respectively. (c) Propagation loss as a function of wavelength.

5. Conclusion

In conclusion, we have reported a promising method to fabricate high crystalline quality polycrystalline silicon waveguides suitable for application across the near-to-mid-infrared regimes. The waveguides were produced using deposition temperatures of only 230°C, followed by a localized laser heat treatment, making them compatible with CMOS fabrication processing. Transmission losses below 3 dB cm⁻¹ were obtained at 1.55 μm as well as across the wavelength range of 2 – 2.25 μm, which we attribute to the high quality polycrystallinity and very smooth surfaces enabled by the melting and reshaping of the waveguides during the laser processing. The results indicate that polycrystalline silicon waveguides could find numerous applications for the development of integrated optoelectronic systems with extended operation into the mid-infrared wavelength range.

Funding. Engineering and Physical Sciences Research Council (EP/M022757/1, EP/N013247/1, EP/P000940/1).

Disclosures. The authors declare no conflicts of interest.

Data availability. Data underlying the results presented in this paper are available in [26].

References

1. F. Dell'Olio and V. M. N. Passaro, "Optical sensing by optimized silicon slot waveguides," *Opt. Express* **15**(8), 4977–4993 (2007).
2. J. Brosi, C. Koos, L. C. Andreani, M. Waldow, J. Leuthold, and W. Freude, "High-speed low-voltage electro-optic modulator with a polymer-infiltrated silicon photonic crystal waveguide," *Opt. Express* **16**(6), 4177–4191 (2008).
3. C. Koos, "All-optical high-speed signal processing with silicon-organic hybrid slot waveguides," *Nat. Photonics* **3**(4), 216–219 (2009).
4. N. Sherwood-Droz and M. Lipson, "Scalable 3D dense integration of photonics on bulk silicon," *Opt. Express* **19**(18), 17758–17765 (2011).
5. B. Kuyken, X. Liu, R. M. Osgood, R. Baets, G. Roelkens, and W. M. Green, "A silicon-based widely tunable short-wave infrared optical parametric oscillators," *Opt. Express* **21**(5), 5931–5940 (2013).
6. R. Takei, S. Manako, E. Omoda, Y. Sakakibara, M. Mori, and T. Kamei, "Sub-1 dB/cm submicrometer-scale amorphous silicon waveguide for backend on-chip optical interconnects," *Opt. Express* **22**(4), 4779–4788 (2014).
7. G. T. Reed, "The optical age of silicon," *Nature* **427**(6975), 595–596 (2004).
8. R. L. Espinola, J. I. Dadap, R. M. Osgood, S. J. McNab, and Y. A. Vlasov, "C-band wavelength conversion in silicon photonic wire waveguides," *Opt. Express* **13**(11), 4341–4349 (2005).
9. Y. H. D. Lee, M. O. Thompson, and M. Lipson, "Deposited low temperature silicon GHz modulator," *Opt. Express* **21**(22), 26688–26692 (2013).
10. A. H. Atabaki, S. Moazeni, F. Pavanello, H. Gevorgyan, J. Notaros, L. Alloatti, M. T. Wade, C. Sun, S. A. Kruger, H. Meng, K. Al Qubaisi, I. Wang, B. Zhang, A. Khilo, C. V. Baiocco, M. A. Popovic, V. M. Stojanovic, and R. J. Ram, "Integrating photonics with silicon nanoelectronics for the next generation of systems on a chip," *Nature* **556**(7701), 349–354 (2018).
11. B. Kuyken, H. Ji, S. Clemmen, S. K. Selvaraja, H. Hu, M. Pu, M. Galili, P. Jeppesen, G. Morthier, S. Massar, L. K. Oxenløwe, G. Roelkens, and R. Baets, "Nonlinear properties of and nonlinear processing in hydrogenated amorphous silicon waveguides," *Opt. Express* **19**(26), B146–B153 (2011).
12. Y. Franz, A. F. J. Runge, S. Z. Oo, G. Jimenez-Martinez, N. Healy, A. Khokhar, A. Tarazona, H. M. H. Chong, S. Mailis, and A. C. Peacock, "Laser crystallized low-loss polycrystalline silicon waveguides," *Opt. Express* **27**(4), 4462–4470 (2019).
13. S. Zhu, G. Q. Lo, J. D. Ye, and D. L. Kwong, "Influence of RTA and LTA on the optical propagation loss in polycrystalline silicon wire waveguides," *IEEE Photonics Technol. Lett.* **22**(7), 480–482 (2010).
14. O. Aktas, S. J. MacFarquhar, S. Z. Oo, A. Tarazona, H. M. H. Chong, and A. C. Peacock, "Nonlinear properties of laser-processed polycrystalline silicon waveguides for integrated photonics," *Opt. Express* **28**(20), 29192–29201 (2020).
15. P. Y. Yang, S. Stankovic, J. Crnjanski, E. J. Teo, D. Thomson, A. A. Bettiol, M. B. H. Breese, W. Headley, C. Giusca, G. T. Reed, and G. Z. Mashanovich, "Silicon photonic waveguides for mid- and long-wave infrared regions," *J. Mater. Sci. Mater. Electron.* **20**(S1), 159–163 (2009).
16. R. Soref, "Mid-infrared photonics in silicon and germanium," *Nat. Photonics* **4**(8), 495–497 (2010).
17. G. Z. Mashanovich, M. M. Milosevic, M. Nedeljkovic, N. Owens, B. Xiong, E. J. Teo, and Y. Hu, "Low loss silicon waveguides for the mid-infrared," *Opt. Express* **19**(8), 7112–7119 (2011).
18. V. Lindroos, M. Tilli, A. Lehto, and T. Motooka, *Handbook of silicon based MEMS materials and technologies*, (Elsevier, 2010).
19. A. H. Mahan, J. Carapella, B. P. Nelson, R. S. Crandall, and I. Balberg, "Deposition of device quality, low H content amorphous silicon," *J. Appl. Phys.* **69**(9), 6728–6730 (1991).

20. K. F. Feenstra, R. E. Schropp, and W. F. Van DerWeg, "Deposition of amorphous silicon films by hot-wire chemical vapor deposition," *J. Appl. Phys.* **85**(9), 6843–6852 (1999).
21. R. E. Schropp, "Hot wire chemical vapor deposition: recent progress, present state of the art and competitive opportunities," *ECS Trans.* **25**(8), 3–14 (2009).
22. S. Z. Oo, A. Tarazona, A. Z. Khokhar, R. Petra, Y. Franz, G. Z. Mashanovich, G. T. Reed, A. C. Peacock, and H. M. H. Chong, "Hot-wire CVD low-loss a-Si:H waveguides for silicon photonic devices," *Photonics Res.* **7**(2), 193–200 (2019).
23. N. Healy, S. Mailis, N. M. Bulgakova, P. J. Sazio, T. D. Day, J. R. Sparks, H. Y. Cheng, J. V. Badding, and A. C. Peacock, "Extreme electronic bandgap modification in laser-crystallized silicon optical fibres," *Nat. Mater.* **13**(12), 1122–1127 (2014).
24. C.-Y. Peng, C.-F. Huang, Y.-C. Fu, Y.-H. Yang, C.-Y. Lai, S.-T. Chang, and C. W. Liu, "Comprehensive study of the Raman shifts of strained silicon and germanium," *J. Appl. Phys.* **105**(8), 083537 (2009).
25. O. Aktas and A. C. Peacock, "Laser thermal processing of group IV semiconductors for integrated photonic systems," *Adv. Photonics Res.* **2**(7), 2000159 (2021).
26. A. N. Ghosh, S. J. Macfarquhar, O. Aktas, T. S. Saini, S. Z. Oo, H. M. H. Chong, and A. C. Peacock, "Dataset for the journal paper titled "Low-temperature polycrystalline silicon waveguides for low loss transmission in the near-to-mid-infrared region"," University of Southampton (2022), <https://doi.org/10.5258/SOTON/D2332>.